WILEY-VCH

Supplementary Information for

Multifunctional Ultra-Wide-Angle Spatial Optical Analog Computing in the Terahertz Regime

Yongliang Liu, Bo Yu, Lesiqi Yin, Wenwei Liu, Qi Liu, Yifei Xu, Minghui Deng, Zhancheng Li, Cheng Gong*, Hua Cheng* and Shuqi Chen**

Y. Liu, B. Yu, W. Liu, Q. Liu, Y. Xu, Z. Li, H. Cheng, S. Chen
The Key Laboratory of Weak Light Nonlinear Photonics, Ministry of Education, School of Physics and TEDA Institute of Applied Physics, Nankai University, Tianjin 300071, China
E-mail: wliu@nankai.edu.cn; hcheng@nankai.edu.cn; schen@nankai.edu.cn

L. Yin, M. Deng and C. Gong
Institute of Modern Optics, Nankai University, Tianjin Key Laboratory of Micro-scale Optical Information Science and Technology, Tianjin, 300350, China
E-mail: gongcheng@nankai.edu.cn

C. Gong
Academy for Advanced Interdisciplinary Studies, Nankai University, Tianjin, 300350, China

S. Chen
School of Materials Science and Engineering, Smart Sensing Interdisciplinary Science Center, Nankai University, Tianjin 300350, China

S. Chen
The Collaborative Innovation Center of Extreme Optics, Shanxi University, Taiyuan 030006, China

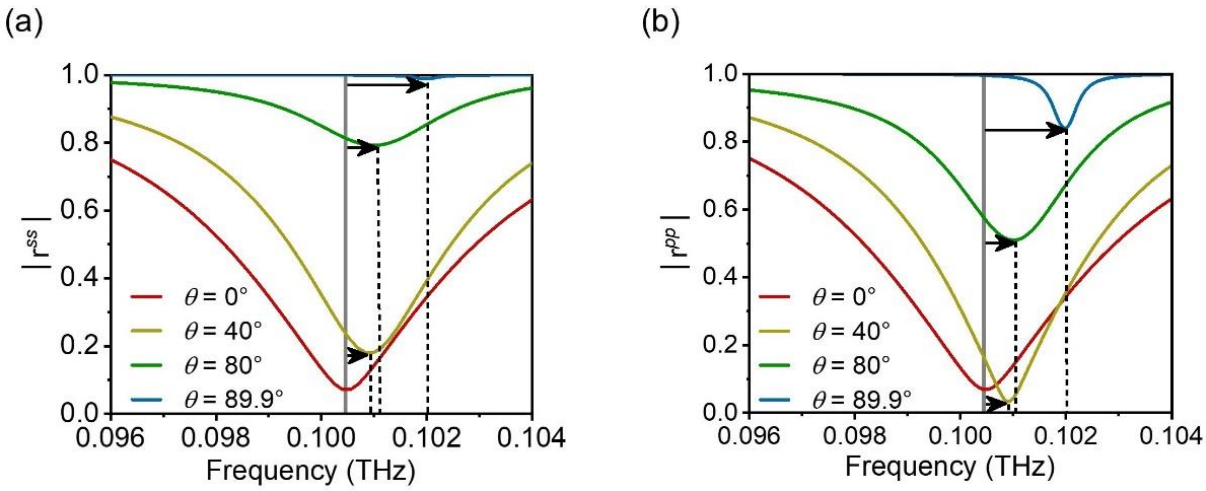

Figure S1. The reflection spectra of the metasurface for (a) *s*- and (b) *p*-polarized at different incident angles.

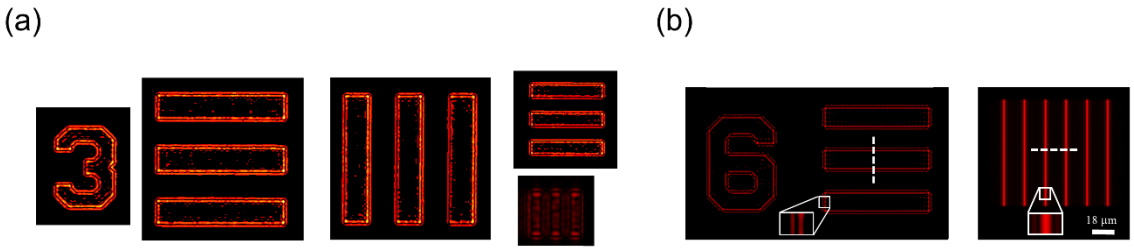

Figure S2. Reconstructed images obtained by applying the experimentally measured transfer functions from (a) Ref. [25] and (b) Ref. [41] for the same input image.

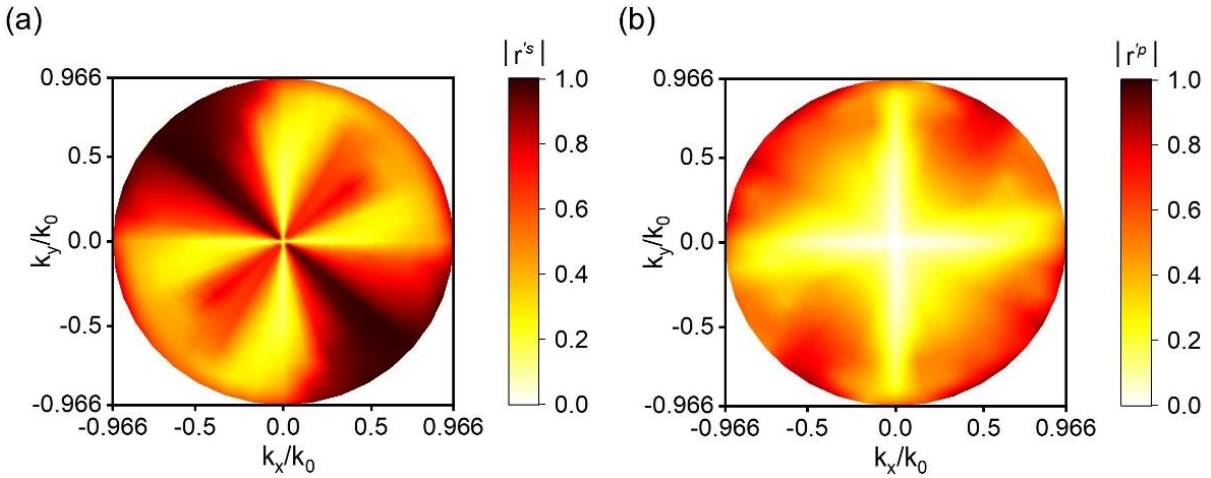

Figure S3. Experimental two-dimensional transfer functions of the metasurface for (a) *s*- and (b) *p*-polarized incident incidence.

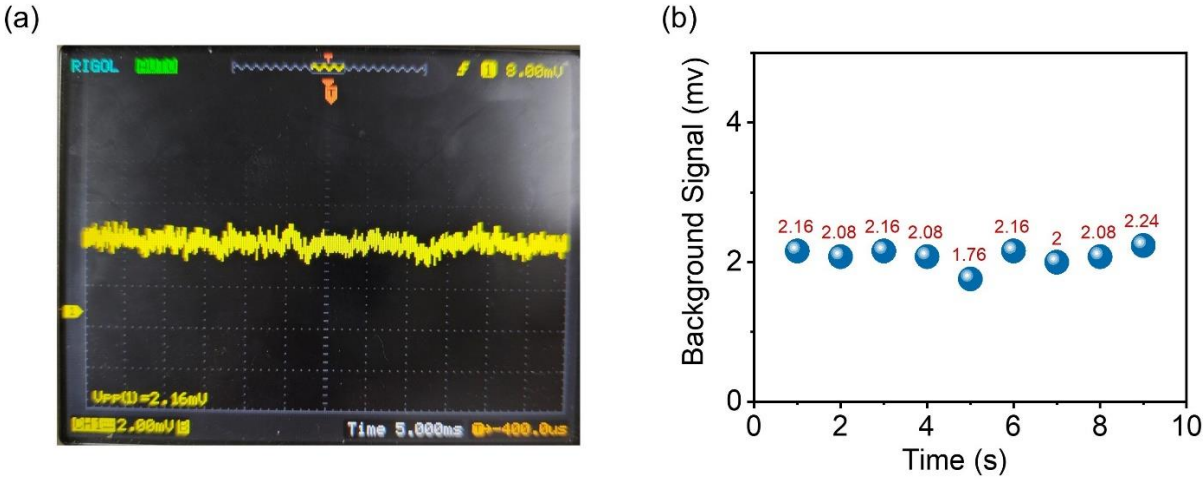

Figure S4. (a) The real-time oscilloscope measurement of the background signal. (b) Time-dependent background signal recorded over 10 seconds, with individual measurements indicated in blue and corresponding values labeled in red.

Table S1 Measured and simulated results under *s*-polarization.

θ	metal	sample	S_{11} (measured)	S_{11} (simulated)
0°	68 mV	2.4 mV	0.07	0.072
30°	660 mV	20 mV	0.165	0.172
45°	440 mV	34 mV	0.27	0.295
60°	236 mV	42 mV	0.413	0.46
75°	72 mV	35 mV	0.686	0.701

Table S2 Measured and simulated results under *p*-polarization.

θ	metal	sample	S_{11} (measured)	S_{11} (simulated)
0°	72 mV	2.6 mV	0	0
30°	470 mV	12 mV	0.0728	0.065
45°	376 mV	16 mV	0.1365	0.142
60°	320 mV	20 mV	0.2052	0.235
75°	150 mV	56 mV	0.58342	0.421

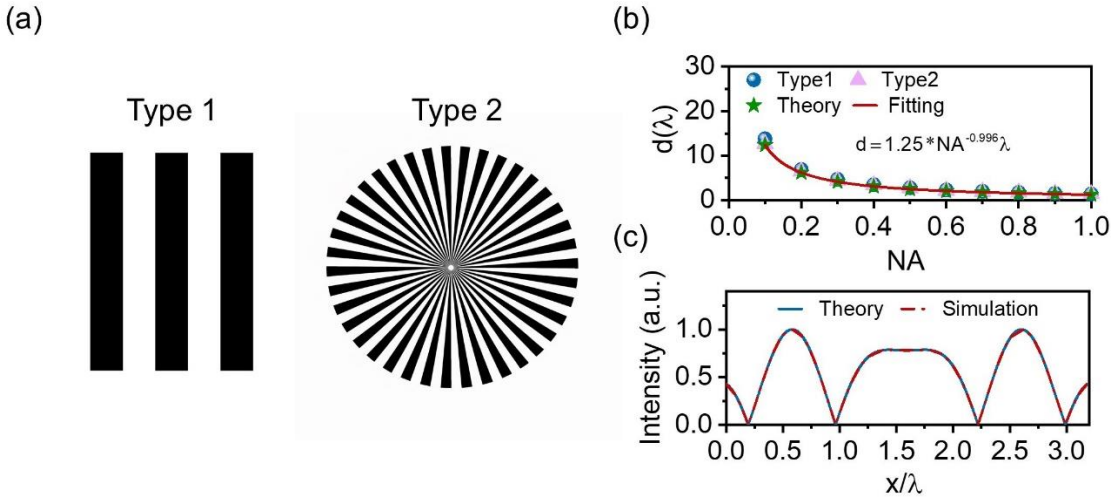

Figure S5. (a) Different types of targets as the input object. (b) Dependence of the edge-detection resolution limit on NA for different object types. (c) The theoretical and calculated edge-image distributions for NA = 1.

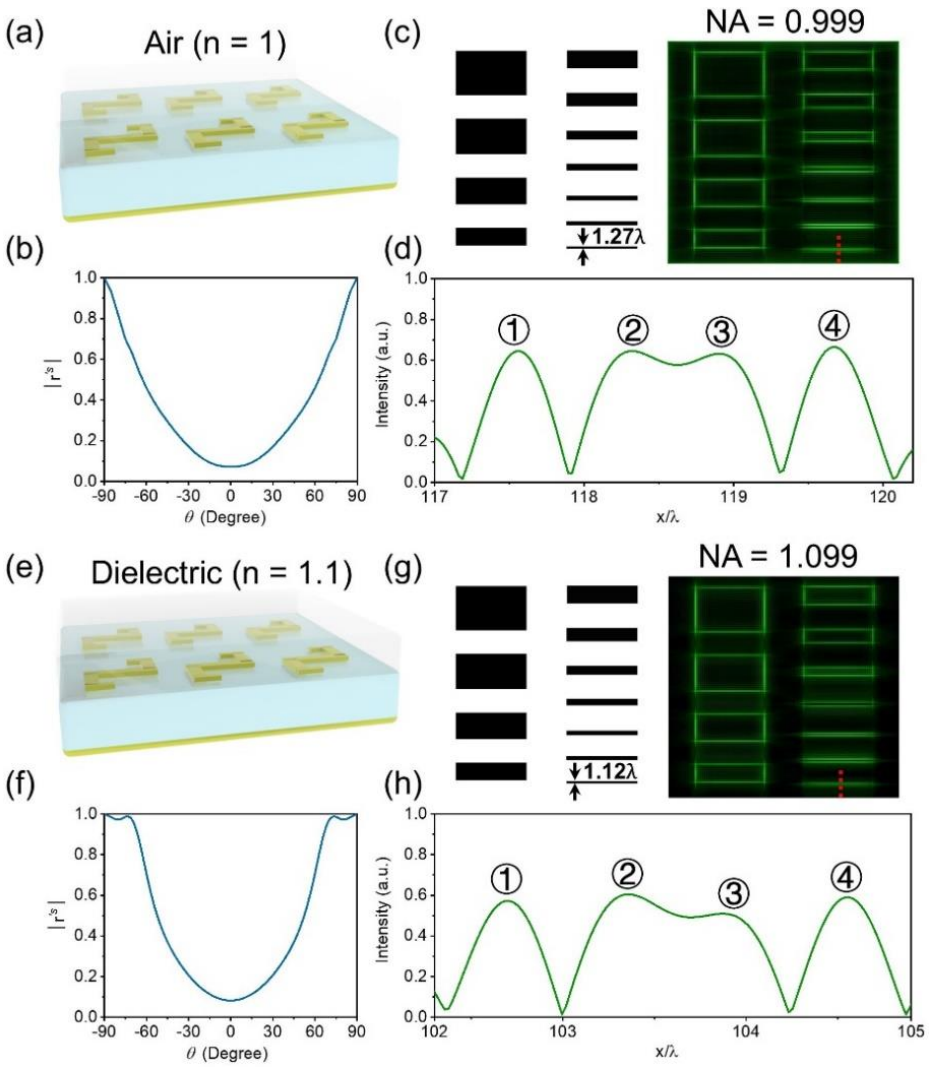

Figure S6. (a), (e) Metasurface embedded in air (n = 1) and in a dielectric medium (n = 1.1), respectively. (b), (f) Simulated optical transfer function for the second-order differentiation

under different dielectric environments, respectively. (c), (g) The original image and the processed image with different NA, respectively. (d), (h) Vertical-cut intensity of the differentiated images along the red dashed line in panels (c), (g), indicating that the minimum resolvable feature size improves from 1.27λ to 1.12λ, confirming the enhancement of edge-detection resolution.